Applied Physics A (2018) 124:647
https://doi.org/10.1007/s00339-018-2074-7

Applied Physics A
Materials Science & Processing

Ion- and electron-beam-induced structural changes in cubic yttria-stabilized zirconia

Miyoko Tanaka[1]

Received: 11 July 2018 / Accepted: 28 August 2018 / Published online: 28 August 2018

Abstract
Thin yttria-stabilized zirconia (YSZ) (100) transmission electron microscopy (TEM) samples prepared using 5 kV Ar ion sputtering and subsequent annealing with 5 kV electron beams under ultrahigh vacuum (UHV) environment were observed with TEM. A new phase which is electron conducting and has high electron beam tolerance is formed. The phase grows epitaxially with the YSZ matrix and has a cubic structure. It is estimated that substrate YSZ reacted with surface contaminants to from ZrC during electron beam annealing. When the substrates were thoroughly cleaned before ion beam irradiation, no new phase formation was observed. Instead, formation of faceted holes was identified.

1 Introduction

Yttria-stabilized zirconia (YSZ) is a material with high hardness, refractoriness, low thermal conductivity, and high ion conductivity. These distinctive characters make it widely used for thermal barrier coating, gas sensors, and solid oxide fuel cells [1–4]. It also attracts great attention for the use in radiation environment due to its high fracture toughness and radiation tolerance [5, 6]. For these reasons, many ion and electron beam irradiation studies have been carried out to clarify its properties under irradiation and their mechanisms as well as to modify its relevant properties [5–7]. Hence these studies are mainly performed with high energy beams (100 keV or higher).

Compared to these swift irradiation studies, only limited number of works dealt with irradiation of low energy beams (several keV or lower). However, since low energy beams are generated subsidiary and constantly with the presence of higher energy ones, it is necessary to investigate the behavior of low energy beams and their effects on the material as well. So far, several groups investigated irradiation process by low energy beams and resultant reduction of YSZ. Simpson et al. found that O^+ is the primary ionic desorption product during low-energy (0.5–3 kV) electron bombardment [8]. Igno et al. reported that reduction of the YSZ target start to be observed when the energy of the irradiating Ar ions is higher than 1 keV [9]. Cotter et al. found that with 2 keV electrons oxygen loss is accompanied by specific reduction Zr(IV) to Zr(0) without concomitant reduction of Y(III) [10]. However, sequential or multiple irradiation, which often occurs in real cases, has not been investigated yet.

In the present study, we investigated radiation effects of low energy ion and electron beams on YSZ crystals. Thin YSZ (100) samples that were treated with low energy Ar^+ ion and electron beams were observed with transmission electron microscopy (TEM). Both beams induced structural changes to the samples, and a new phase formation was promoted in some cases. The identification of the new phase and its formation mechanism will be discussed.

2 Experiments

YSZ single crystals with the (100) orientation for 9.4–10 atomic % Y_2O_3 (Crystal Base Co. Ltd.) were used in this study. Thin TEM samples were prepared by mechanical thinning, dimpling and ion milling using 5 kV Ar^+ beams (GATAN PIPS 691). The ion beams were irradiated at an incident angle of 80 degrees for about 180 min, and the beam current was about 10 μA on average. This ion milling process simultaneously functions as low energy ion irradiation, so we regard it as ion irradiation in the present study.

Ion milled samples were then introduced into an ultrahigh vacuum (UHV) chamber attached to a UHV-TEM and

✉ Miyoko Tanaka
TANAKA.Miyoko@nims.go.jp

[1] Research Center for Advanced Measurement and Characterization, National Institute for Materials Science, Tsukuba 305-0003, Japan

irradiated with electron beams using an accelerating voltage of 5 kV and a beam current of about 1 mA (Omegatron OME-0050LRH). This irradiation process also acts as sample annealing. Temperature rise due to this process was about 1100 K. Considering the measurement error of the pyrometer (which is typically about 50 K) and the local temperature gradient due to sample geometry, the actual temperature is estimated to range from 1000 to 1200 K.

After electron beam irradiation, samples were transferred to the TEM (JEM-2000VF, JEOL) without breaking vacuum to avoid any artifact. TEM was operated at an accelerating voltage of 200 kV. TEM images and diffraction patterns were recorded to imaging plates. High resolution images were recorded to a CCD camera (GATAN Orius SC200).

3 Results and discussion

3.1 TEM Observation after ion beam irradiation

As received YSZ crystals were whitish transparent. Their color did not change through mechanical thinning and dimpling. After ion milling, the sample color became dark grey. This kind of "sample darkening" is commonly observed when YSZ crystals are sintered in reducing atmosphere as well as by ion, electron or photon irradiation and electrolysis [11–15]. This will be discussed later.

The samples suffered radiation damage during ion milling. Formation of crystal defects was recognized as in TEM image in Fig. 1a. Partial amorphization near the sample edge was also observed and identified in diffraction pattern from the corresponding area (Fig. 1b), although the cubic YSZ features remained unchanged.

Ar ion milling is a conventional TEM sample preparation method typically used for semiconductors and ceramics. It uses Ar ions to physically sputter out the substrate atoms to electron transparent thickness. Although being quite useful, it inevitably produces lattice damage and artifacts [16]. In the present case, lattice damage occurs simultaneously

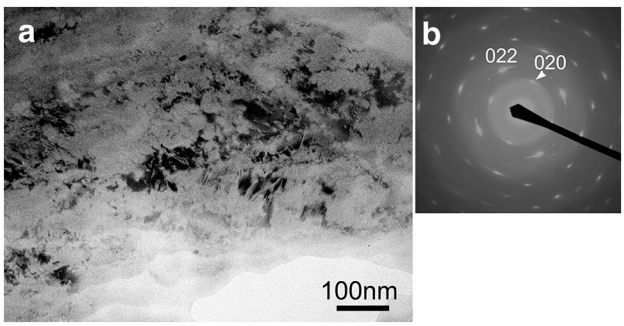

Fig. 1 As prepared YSZ(100) TEM sample. **a** TEM image showing radiation damage and **b** corresponding diffraction pattern

with sputtering. The mean implantation depths (projected ranges Rp) of Ar ions simulated by SRIM code [17] is about 5.1 nm. Since the final thickness of the thin regions after ion milling is typically around 10–20 nm, Ar ions can reach the depth of up to half of the sample thickness.

Contrary to what was expected before experiment, most TEM observation was not interrupted by accumulation of static electric charges, or the charging effect [18, 19]. It is a phenomenon commonly seen while observing insulating materials with TEM or scanning electron microscopy (SEM). Instead of getting shaky or wobbling images due to the charging effect, "calm" TEM observation was possible most of the times. No obvious charging was recognized during normal observation. When focused electron beams (about 2–3 nm in diameter) were irradiated for about 10 s, the local charging and resultant trembling of the specimen started. The trembling continued for a few min even after the electron beam was widened to regular observation mode. These facts imply that the samples gained semi-insulating (or semi-conducting) property after ion milling.

As mentioned above, the sample color changed to dark grey after ion milling. Sample darkening of YSZ is generally explained by removal of oxygen atoms from stoichiometry [11–15]. When oxygen vacancies are formed by some manner, they are populated by electrons that cause dark color like free electrons do in metals. Deficiency of oxygen can be introduced by simple annealing, electric currents, electrolysis, photolysis, or irradiation of ions or electrons [11–15]. Taking these background and results suggesting oxygen desorption by low-energy ion or electron beam irradiation [8–10], YSZ samples in the present study are assumed to have lost oxygen atoms to some amount during ion milling, which resulted in semi-insulating character and calm TEM observation.

3.2 TEM observation after electron beam irradiation

Electron beam irradiation to samples in a UHV chamber turned the color into black. It also changed the morphology and structure of the samples drastically. Figure 2a shows a TEM image of a sample near the edge area. Distinct features are formation of protrusions at the edge region and moiré fringes that cover almost all area but protrusions. Diffraction pattern from the area with moiré fringes is shown in Fig. 2b. The pattern clearly presents that a new phase is formed on the sample and interferes with the YSZ matrix. The formation mechanism of protrusions will be discussed later.

High resolution TEM (HRTEM) images from the inner area away from the edge region where no moiré fringes exist (not at protrusion) show lattice images of YSZ{200} planes with a plane spacing of about 0.26 nm (Fig. 3a, the right-hand side). On the contrary, HRTEM images from

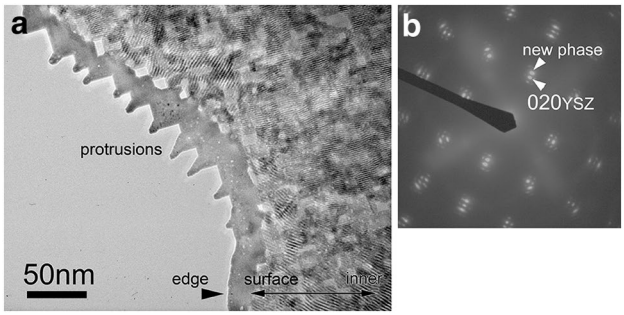

Fig. 2 YSZ(100) sample after electron beam irradiation. **a** TEM image showing formation of a new phase and **b** corresponding diffraction pattern

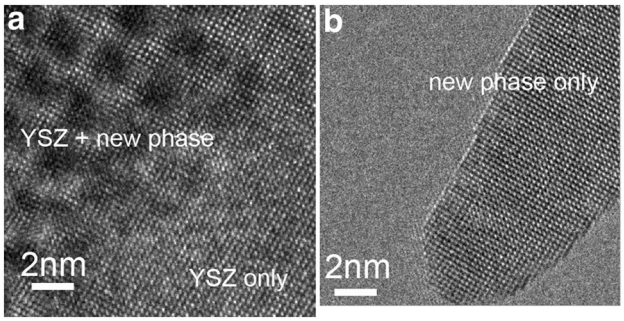

Fig. 3 HRTEM micrographs of YSZ(100) sample. **a** HRTEM image from the inner region showing moiré fringes formed with the matrix and the new phase. The right-hand side shows lattice fringes of the matrix. **b** HRTEM image from the edge area only showing the new phase

the protrusions differ from these images (Fig. 3b). They do show two sets of lattice fringes of the same spacings that are normal to one another, i.e., {200} planes of cubic structure. However, the spacing of the planes was measured as about 0.23 nm, and did not match those of YSZ ones. HRTEM images and diffraction patterns from area with moiré fringes (Fig. 3a, the left-hand side and Fig. 2b) reveal that the fringes arise from the interaction between YSZ < 200 > reflections and those of the new phase. Namely, the phase grows epitaxially on the YSZ substrate.

These results imply that electron beam annealing changes some part of the YSZ matrix into a new phase. Since only the new phase was identified at the edge protrusions, it is likely that the new phase grows from the surfaces of the samples to inward, consuming the underlying YSZ substrate. As the edge area of TEM samples is thin, the entire substrate matrix turned into the new phase. The area away from the edge must have a layered structure with the new phase on front and/or back surfaces.

Contrary to what was seen with samples before electron beam annealing, annealed samples did not show any charging effect even with focused electron beam irradiation for more than 5 min. This fact implicates that the certain part of the samples become electron conducting. Obviously, the new phase should have this character.

Now the point is what the new phase is. Since it has a conducting character, it should not be insulating ZrO_2 or Y_2O_3. Among other Zr compounds and pure Zr/Y, including metastable ZrO and ZrC_xO_y [20, 21], the one that has a cubic structure and the lattice constant of 0.46–047 nm corresponds only to ZrC. The original YSZ samples off course did not contain carbon. However, since TEM samples are glued to glass plates with bonding wax (which is organic compounds) during sample preparation [22], they usually have certain amount of carbon or hydrocarbon on their surfaces after preparation. These substances are called contaminants. The residual gas inside ion milling chamber could be another source of contaminants. In the present study, it is most likely that surface contaminants reacted with the YSZ substrate during electron beam irradiation and formed ZrC. Formation of ZrC due to the surface contaminant is sometimes observed for YSZ substrates that are annealed at high temperatures [23]. Assuming the new phase to be ZrC, the growth orientation relationship can be written as:

(001) YSZ // (001) ZrC,

[100] YSZ // [100] ZrC.

If we assume the existence of 1 nm organic compounds on sample surfaces, contaminant material (mainly carbon) could be injected into some depth from the surface even with low energy ion irradiation. SRIM estimation provides ion implantation depths of 4.4 nm in this case, with C-atom-distribution spreading into the substrate matrix. The distribution of injected carbon atoms should not be uniform considering the nature of contamination, resulting in random distribution of sets of moiré fringes. The overall process is schematically illustrated in Fig. 4.

Temperature during electron beam irradiation is estimated to be about 1000–1200 K. On the basis of the thermodynamical data of the JANAF table [24], volatility diagram for the Zr/O/C at 1000 and 1200 K as a function of oxygen partial pressure is drawn as Fig. 5. Here we used equilibrium constants of pure ZrO_2 due to the lack of data of YSZ. Since volatility diagrams are not phase diagrams but only representing graphical solutions of various gas–solid reactions [25, 26], it shows simple carbothermal reduction of zirconia,

$$ZrO_2 + 3C = ZrC + 2CO \quad (1)$$

can be achieved in certain conditions. This reduction reaction is one of the most common industrial processes for synthesizing ZrO_2, and currently performed at around

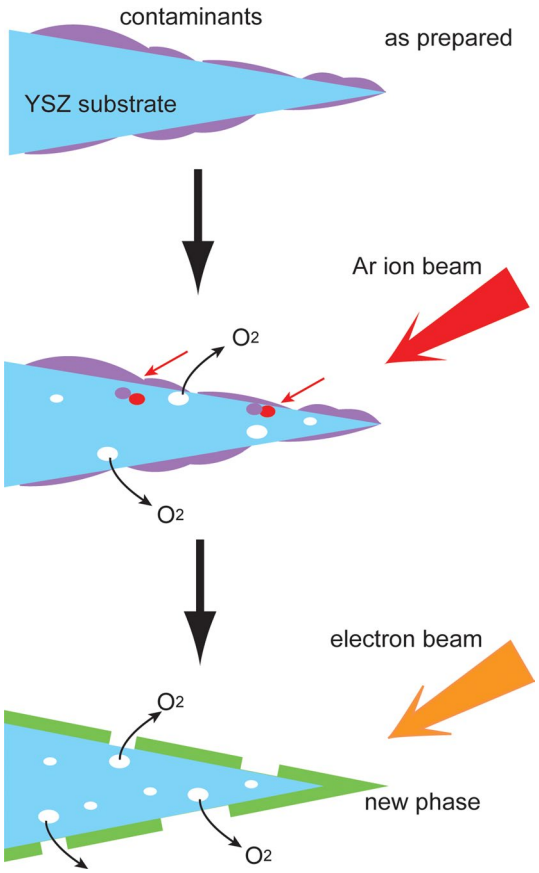

Fig. 4 Schematic drawing of the phase formation procedure

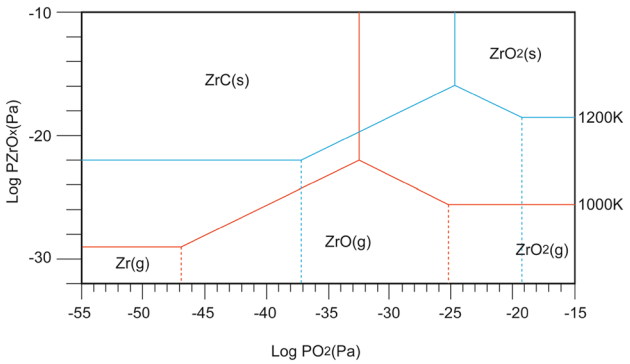

Fig. 5 Volatility diagram for the system Zr/C/O at 100 and 1200 K as a function of partial pressure of oxygen

1800 K [27]. The diagram implies that the reaction temperature can be lowered to the levels of the present annealing if the oxygen partial pressure is as low as -10^{-25} Pa.

Although the actual partial pressure of oxygen inside the UHV chamber is not be able to be measured due to the detection limit of our residual mass spectrometer [28], it is unlikely that the partial pressure goes down so low. Still, the number of residual oxygen atoms is quite limited and other factors such as ion beam mixing of carbon atoms into YSZ substrates could promote reaction (1) and hence ZrC formation.

Similar carbothermal reaction of metal oxide was reported previously. Agrawal et al. have observed transformation of nanocrystalline anatase TiO_2 into TiC by annealing in TEM [29]. In their case, TiO_2 nanocrystals reacted with carbon grid material at about 1300 K. They attributed the reaction to the effect of the electron beam during observation and the vacuum conditions of the microscope. In the meantime, Rankin et al. did in situ heating of ZrO_2 (a mixture of tetragonal and monoclinic phases) powder on carbon grid at 1373K [30]. They only observed sintering and surface fluctuation but no new phase formation. The difference in these two studies may come from the difference in experimental conditions such as particle sizes, vacuum conditions and sample preparation methods, as well as the different thermodynamic characters. In our case, even though the reaction temperature was lower than these studies, the new phase formation was observed. Since we used crystalline substrates and UHV environment, structural modification during ion and electron beams irradiation and the low partial pressure of oxygen are most likely to promote the reaction.

3.3 Irradiation to thoroughly cleaned samples

To assess the effect of contamination on the new phase formation, some of the samples were thoroughly cleaned in acetone for several days before Ar ion milling. They were then treated the same way as other samples. The amount of contamination left on the surface of the samples is expected to become smaller in this case. After electron beam irradiation, new phase formation was hardly observed on those samples. Instead, formation of many faceted holes was identified. Figure 6a shows these holes aligned near a sample edge. Corresponding diffraction pattern (Fig. 6b) clearly reveals the existence of only the YSZ substrate. This type of hole formation is typically observed with electron beam

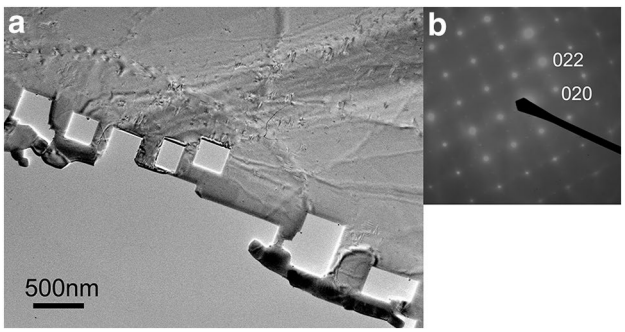

Fig. 6 **a** TEM micrograph of YSZ (100) sample which was thoroughly cleaned before beam treatment, showing formation of faceted holes. **b** Corresponding diffraction pattern

irradiated transition-metal oxide materials at elevated temperature and is attributed mainly to physical sputtering [31]. At elevated temperature, thermally assisted surface diffusion promotes the growth of faceting of surfaces of sputter pits to develop into holes that consist of low surface energy planes. Since the distribution of carbon compounds was expected to be random, sputtering and successive hole formation must have occurred where little carbon atoms existed. The formation of protrusions at the sample edges described in Sect. 3.2 can be explained by this mechanism. At first, sputter pits are formed by electron beam irradiation where there are little carbon atoms existed. They grow anisotropically to develop into faceted holes for longer irradiation. These edges of the facets are predominantly {110} planes. When the thinnest edges break, protrusions are left at the edges.

The present results could be beneficial to some fields. The fact that clean YSZ is susceptible to sputtering suggests that cautious environmental setting is required in irradiation fields. At the same time, a new approach to form that protective layer on YSZ which prevent sputtering would be developed with more controllability of the new phase formation. More detailed analysis of the new phase and optimization of formation conditions are being planned at the moment.

4 Conclusions

Thin YSZ (100) samples were treated with 5 kV ion and electron beams. A new phase was formed after the treatments. The phase has a cubic structure with a lattice parameter of about 0.46 nm. The phase seems to grow epitaxially on YSZ matrix. Only the new phase was identified at the edge region. The phase has a high tolerance to focused electron beam irradiation. It is estimated that surface contaminant reacted with substrate matrix and formed ZrC. UHV environment and both ion and electron beam irradiation are assumed to promote this reaction. The samples completely cleaned before beam irradiation did not show new phase formation but growth of faceted holes, indicating that contaminant played a key role in the new phase formation.

References

1. B.A. Boukamp, The amazing perovskite anode. Nat. Mater. **2**, 294–296 (2003)
2. R. Vaßen, M.O. Jarligo, T. Steinke, D.E. Mack, D. Stöver, Overview on advanced thermal barrier coatings. Surf. Coat. Tech. **205**, 938–942 (2010)
3. N. Miura, M. Nakatou, S. Zhuiykov, Impedancemetric gas sensor based on zirconia solid electrolyte and oxide sensing electrode for detecting total NO_x at high temperature. Sens. Actuators B **93**, 221–228 (2003)
4. M.N. Tsampas, F.M. Sapountzi, P. Vernoux, Applications of yttria stabilized zirconia (YSZ) in catalysis. Cat. Sci. Tech. **5**, 4884–4900 (2015)
5. P. kalita, S. Ghosh, G. Sattonnay, U.B. Singh, V. Grover, R. Shukla, S. Amirthapandian, R. Meena, A.K. Tyagi, D.K. Avasthi, Role of temperature in the radiation stability of yttria stabilized zirconia under swift heavy ion irradiation: a study from the perspective of nuclear reactor applications. J. Appl. Phys. **122**, 025902 (2017)
6. G. Velişa, A. Debelle, L. Thomé, S. Mylonas, L. Vincent, A. Boulle, J. Jagielski, D. Pantelica, Implantation of high concentration noble gases in cubic zirconia and silicon carbide: a contrasted radiation tolerance. J. Nucl. Mat. **451**, 14–23 (2014)
7. U. Vohrer, H.–D. Wiemhfer, W. Göpel, B.A. von Hassel, A.J. Burggraaf, Electronic properties of ion-implanted yttria-stabilized zirconia. Solid State Ionics **59**, 141–149 (1993)
8. W.C. Simpson, W.K. Wang, J.A. Yarmoff, T.M. Orlando, Photon- and electron-stimulated desorption of O^+ from zirconia. Surf. Sci. **423**, 225–231 (1999)
9. G.M. Ingo, G. Marletta, Ion beam induced reduction of metallic cations in yttria-zirconia. Nucl. Inst. Met. Phys. Res. B **116**, 440–446 (1996)
10. M. Cotter, R.G. Egdell, Electron beam reduction of cubic Y-doped ZrO_2(100): a study by X-ray photoelectron spectroscopy. J. Solid State Chem. **66**, 364–368 (1987)
11. J.S. Moya, R. Moreno,, J. Requena, Black color in partially stabilized zirconia. J. Am. Ceram. Soc. **71**, C479–C480 (1988)
12. R.W. Rice, Comment on "Black color in partially stabilized zirconia". J. Am. Ceram. Soc. **74**, 1745–1746 (1991)
13. X. Guo, Y.–Q. Sun, K. Cui, Darkening of zirconia: a problem arising from oxygen sensors in practice. Sens. Actuators B **31**, 139–145 (1996)
14. V.R. Pai Verneker, D. Nagle, Effect of reduction on vickers hardness of stabilized zirconia. J. Mat. Sci. Lett. **9**, 192–194 (1990)
15. D. Nagle, V.R. Pai Verneker, A.N. Petelin, G. Groff, Optical absorption of electrolytically colored single crystals of yttria-stabilized zirconia. Mat. Res. Bull. **24**, 619–623 (1989)
16. D.J. Barber, Radiation damage in ion-millled specimens: characteristics, effects and methods of damage limitation. Ultramic. **52**, 101–125 (1993)
17. J.F. Ziegler, J.P. Biersack, The stopping and range of ions in matter (SRIM, Version 2013)
18. J. Cazaux, Correlations between ionization radiation damage and charging effects in transmission electron microscopy. Ultramic **60**, 411–425 (1995)
19. R.F. Egerton, P. Li, M. Malac, Radiation damage in the TEM and SEM. Micron **35**, 399–409 (2004)
20. R.J. Nicholls, N. Ni. S. Lozano-Perez, A. London, D.W. McComb, P.D. Nellist, C.R.M. Grovenor, C.J. Pichard, J.R. Yates, Crystal structure of the ZrO phase at zirconium/zirconium oxide interfaces. Adv. Eng. Mat. **17**, 211–215 (2015)
21. G. Velişa, S. Mylonas, P. Trocellier, L. Thomé, A. Debelle, S. Vaubaillon, C. Bachelet, Ion beam syntheses of ZrCxOy nanoparticles in cubic zirconia. J. Appl. Phys. **119**, 165902 (2016)
22. J.J. Hren, Specimen contamination in analytical electron microscopy: sources and solutions. Ultramic **3**, 375–380 (1979)
23. R.G. Green, L. Barré, J.B. Giorgi, Nano-structures in YSZ(100) surfaces: implication for metal deposition experiments. Surf. Sci. **601**, 792–802 (2007)
24. M.W. Chase, N.I.S.T.-J.A.N.A.F. Thermochemical, Am Ceram Soc and Am Inst Phys. (NIST, Gaithersburg, 1998)
25. A.H. Heuer, V.L.K. Lou, Volatility diagrams for silica, silicon nitride, and silicon carbide and their application to high-temperature decomposition and oxidation. J. Am. Ceram. Soc. **73**, 2789–2803 (1990)

26. P. AMaitre, Lefort, Solid state reaction of zirconia with carbon. Solid State Ionics **104**, 109–122 (1997)
27. D.–W. Lee, S.–M. Jin, J.–H. Yu, H.–M. Lee, Synthesis of ultrafine ZrC powders by novel reduction process. Mater. Trans. **51**, 2266–2268 (2010)
28. M. Tanaka, K. Furuya, M. Takeguchi, T. Honda, Surface observation of Mo nanocrystals deposited on Si (111) thin films by a newly developed ultrahigh vacuum field-emission transmission electron microscope. Thin Solid Films **319**, 110–114 (1998)
29. A. Agrawal, J. Cizeron, V.L. Colvin, In situ high-temperature transmission electron microscopy observation of the formation of nanocrystalline TiC from nanocrystalline anatase (TiO_2). Microsc. Microanal. **4**, 269–277 (1998)
30. J. Rankin, B.W. Sheldon, In situ TEM sintering of nano-sized ZrO_2 particles. Mater. Sci. Eng. A **204**, 48–53 (1995)
31. M.R. MacCartney, D.J. Smith, Studies of electron irradiation and annealing effects on TiO_2 surfaces in ultrahigh vacuum using high-resolution electron microscopy. Surf. Sci. **250**, 169–178 (1991)